frontiers | Frontiers in Oncology

TYPE Original Research
PUBLISHED 22 August 2022
DOI 10.3389/fonc.2022.855519

OPEN ACCESS

EDITED BY
Marie-France Penet,
Johns Hopkins Medicine, United States

REVIEWED BY
Durgesh K. Dwivedi,
King George's Medical University, India
William Ian Duncombe Rae,
The University of Sydney, Australia

*CORRESPONDENCE
Michał Lis
lis.michal.md@gmail.com

†These authors have contributed equally to this work and share first authorship

‡These authors have contributed equally to this work and share last authorship

SPECIALTY SECTION
This article was submitted to Breast Cancer, a section of the journal Frontiers in Oncology

RECEIVED 15 January 2022
ACCEPTED 11 July 2022
PUBLISHED 22 August 2022

CITATION
Dołęga-Kozierowski B, Lis M, Marszalska-Jacak H, Koziej M, Celer M, Bandyk M, Kasprzak P, Szynglarewicz B and Matkowski R (2022) Multimodality imaging in lobular breast cancer: Differences in mammography, ultrasound, and MRI in the assessment of local tumor extent and correlation with molecular characteristics.
Front. Oncol. 12:855519.
doi: 10.3389/fonc.2022.855519

Multimodality imaging in lobular breast cancer: Differences in mammography, ultrasound, and MRI in the assessment of local tumor extent and correlation with molecular characteristics

Bartosz Dołęga-Kozierowski[1†], Michał Lis[2*†], Hanna Marszalska-Jacak[1], Mateusz Koziej[3], Marcin Celer[1], Małgorzata Bandyk[1], Piotr Kasprzak[1‡], Bartłomiej Szynglarewicz[4,5‡] and Rafał Matkowski[4,5‡]

[1]Breast Unit, Department of Breast Imaging, Lower Silesian Oncology, Pulmonology and Hematology Center, Wroclaw, Poland, [2]Burn and Plastic Surgery Department, Ludwik Rydygier Memorial Specialized Hospital in Krakow, Krakow, Poland, [3]Department of Anatomy, Jagiellonian University Medical College, Krakow, Poland, [4]Breast Unit, Department of Breast Surgery, Lower Silesian Oncology, Pulmonology and Hematology Center, Wroclaw, Poland, [5]Department of Oncology, Faculty of Medicine, Wroclaw Medical University, Wroclaw, Poland

Introduction: Invasive lobular breast cancer (ILC) is a diagnostic challenge due to the diversity of morphological features. The objective of the study was to investigate the presentation and local extent of ILC using various imaging techniques and to assess the correlation between imaging and molecular profile.

Materials and methods: We reviewed 162 consecutive patients with ILC found on vacuum-assisted biopsy, who underwent evaluation of the lesion morphology and extent using ultrasound (US), mammography (MMG), and magnetic resonance imaging (MRI). Radiographic features were compared with ILC intrinsic subtype based on the expression of Ki-67 and estrogen, progesterone, and HER2 receptors.

Results: A total of 113 mass lesions and 49 non-mass enhancements (NMEs) were found in MRI. Masses were typically irregular and spiculated, showing heterogeneous contrast enhancement, diffusion restriction, and type III enhancement curve. NMEs presented mainly as the area of focal or multiregional distribution with heterogeneous or clumped contrast enhancement, diffusion restriction, and type III enhancement curve. Lesion extent significantly varied between MRI and MMG/ultrasonography (USG) ($P < 0.001$) but did not differ between MGF and ultrasonography (USG). The larger the ILC, the higher the disproportion when lesion extent in MRI was compared with MMG ($P < 0.001$) and ultrasonography (USG) ($P < 0.001$). In the study group, there were 97 cases of luminal A subtype (59.9%), 54 cases of luminal B HER2– (33.3%), nine cases of luminal B HER2+ (5.5%), and two cases of triple

negative (1.2%). The HER2 type was not found in the study group. We did not observe any significant correlation between molecular profile and imaging.

Conclusion: MRI is the most effective technique for the assessment of ILC local extent, which is important for optimal treatment planning. Further studies are needed to investigate if the intrinsic subtype of ILC can be predicted by imaging features on MRI.

KEYWORDS

breast cancer, invasive lobular carcinoma (ILC), invasive lobular breast cancer, magnetic resonance imaging, multimodality imaging, lobular breast cancer

Background

Breast cancer imaging is constantly evolving and research protocols are continually being modified. The method of highest sensitivity (94% to 99%) for invasive lobular breast cancer (ILC) detection is magnetic resonance imaging (MRI) (1–3). Although ILC accounts for 5% to 15% of all breast cancers (4) due to its course and wide diversity of histopathological, clinical, and radiological images, ILC still presents significant challenge for clinicians specializing in breast oncology (2, 5, 6).

Biological diversity of ILC is reflected in molecular subtypes defined on the basis of standard biomarkers analyzed *via* immunohistochemistry: estrogen receptor (ER), progesterone receptor (PR), and human epidermal growth factor-2 receptor (HER2) as well as the estimation of tumor proliferation index Ki67 that allows risk stratification and implementation of personalized therapies. The modern classification of lobular breast cancer (LBC) includes five subtypes of different molecular profile: luminal A (ER+ and/or PR+, HER2−, Ki67<15%), luminal B (HER2− subtype: ER+ and/or PR+, HER2−, Ki67≥15%; HER2+ subtype: ER+ and/or PR+, HER2+), HER2 type (ER− and PR−, HER2+), and triple negative (TN) breast cancer (7).

Because of their radiological characteristics, lesions that cannot be seen in mammography (MMG) or in ultrasound (US) are revealed to be advanced when they are exhibited in MRI. Moreover, ILC is often multifocal, multicentric, or even bilateral, each of which influences choice of therapeutic procedure. That is why, for many years, MRI has been recognized as a diagnostic standard for ILC as it has the highest sensitivity among the available imaging methods (2, 8–10).

Abbreviations: BPE, background parenchymal enhancement; ER, estrogen receptor; FGT, fibroglandular tissue; HER2, Herceptin receptor; IDC, invasive ductal carcinoma; ILC, invasive lobular carcinoma; Lum A, luminal A; Lum B, luminal B; MMG, mammography; NME, non-mass enhancement; PGR, progesterone receptor; TN, triple negative.

Magnetic resonance imagining is often emphasized as the LBC diagnosis of choice because it can easily detect changes that other methods often cannot (11). One factor influencing MRI's popularity is that lobular carcinoma spreads along milk ducts and the loss of E-cadherins in terminal duct lobular units. This type of growth is characterized by much lower incidence of necrotic changes, hemorrhages, or microcalcifications when compared to ductal carcinoma *in situ* (2, 5, 12, 13).

The correlation between radiological features and molecular profile of the LBC is the subject of extensive research, the results of which do not allow clear conclusions to be drawn due to relatively small study groups (11, 14–17).

Study objectives

1. The assessment of morphology and local extent of ILC in three imaging techniques.
2. The assessment of the correlation between the results of three imaging methods (MMG, US, and MRI) and molecular profile of ILC.

Materials and methods

One hundred sixty-two patients with ILC diagnosis who were treated in the Breast Unit of Wrocław Comprehensive Cancer Centre, Wroclaw, Poland, between September 2016 and February 2020 were subjected to a retrospective analysis of their imaging (MRI, US, and MMG) and histological test results.

The diagnosis of ILC was made according to the following protocol: patients were referred to the Breast Unit of Wrocław Comprehensive Cancer Centre to check a lesion discovered during outpatient US examination. Shortly thereafter, US and MMG were performed in the Wroclaw breast unit. Results were

analyzed by two independent teams of specialists using American College of Radiology Breast Imaging Reporting and Data System, and patients were qualified for percutaneous core needle biopsy. Ultimately, the study included only patients with ILC confirmed in the histopathological examination.

The criteria for exclusion of patients from the study included neoadjuvant chemotherapy, allergy to gadolinium, and other medical contraindications to contrast-enhanced MRI. US and MMG scans were analyzed by three breast radiologists with at least 20 years of professional experience and one assistant with 4 years of professional experience, whereas the breast MRI scans were subjected to independent dual review by radiologists interpreting more than 600 breast MRI scans per year.

Ultrasound

Esaote My Lab Class C ultrasound devices and a 5- to 13-MHz linear probe were used to perform US examinations. The default "breast" preset was used for the analysis of images, which guaranteed repeatability of the tests. In addition, single focusing was used. The test result was prepared according to ACR BI-RADS.

Mammography

Mammographic examination was performed on the Hologic Selenia Dimension system (Hologic, Inc., Bedford, MA) in standard projections in the compression force range of 90N to 140N and then described on the Hologic console with Secure View software according to ACR BI-RADS lexicon. The measurement was performed as follows: round or oval tumor (main lesion – index mass), spiculated lesion (main lesion without projections), and area of high density (borders of the highest saturation area).

The description included isolated alterations of cell architecture and accompanying changes, as well as microcalcifications measured for greatest extent.

Magnetic resonance imaging

MRI of the breast was performed on the Magnetom Avanto Tim Dot 1.5T (Siemens Healthcare, Erlangen, Germany) with a compatible 18-channel diagnostic breast coil. Imaging was performed within 14 days of core needle biopsy and with the patient in the prone position. The tests were conducted according to the following protocol:

T1 HR—slice thickness, 0.7 mm [voxel size: 0.7 × 0.7 × 0.7 mm; SNR (signal-noise ratio), 1.00]; slices per slab, 208; TR, 5.64 ms/TE, 5.64 ms; FoV read, 250 mm; FoV phase, 169.3; bandwidth = 300 Hz; slice gap, 0.14 mm; flip angle, 15°; and a total acquisition time = 2 min 28 s.

T2—slice thickness, 2 mm (voxel size: 0.5 × 0.5 × 2.0 mm; SNR, 1.00); slices, 57; TR, 6,670 ms/TE, 100 ms; FoV read, 250 mm; FoV phase, 168.8; bandwidth = 326 Hz; slice gap, 0.4 mm; flip angle, 150°; and a total acquisition time = 2 min 53 s.

TIRM (Turbo Invertion Recovery Magnitude)—slice thickness, 2 mm (voxel size: 0.7 × 0.7 × 2.0 mm; SNR, 1.00); slices, 57; TR, 7,850 ms/TE, 63 ms; FoV read, 250 mm; FoV phase, 168.8; bandwidth = 334 Hz; slice gap, 0.4 mm; flip angle, 150°; and a total acquisition time = 3 min 24 s.

T1 3D dynamic—matrix, 389 × 256; slice thickness, 1 mm (voxel size: 1 × 1 × 1 mm; SNR, 1.00); slices per slab, 144; TR, 4.42 ms/TE, 1.7 ms; flip angle, 10°; acquisition time of each phase, approximately 55 s (one phase before contrast, six phases after contrast injection).

DWI—b-value, 50/400/800 s/mm^2; slice thickness, 3 mm (voxel size: 1.3 × 1.3 × 3.0 mm; SNR, 1.00); slice numbers, n = 45; TR, 6300 ms/TE, 70 ms; slice gap, 0.6 mm; and a total acquisition time = 3 min 22 s.

The dynamic test was performed with the administration of the contrast agent Dotarem (gadoterate meglumine) at the dose of 0.1 mmol/kg and the flow of 2 ml/s, followed by a rinse with 30 ml of NaCl.

The tests were analyzed by independent radiology specialists (double reading) using Siemens software tool (Brevis MRI), and all lesions were evaluated by the American College of Radiology – BIRADS breast MRI lexicon (Fifth Edition).

For all axial plane acquisitions, the phase encoding direction was from right to left to limit artifacts repeating cardiac and respiratory movement. Moreover, movement artifacts were eliminated by the "Motion Correction" function. "Color mapping" function allowed confirmation of the locations for determining the enhancement curves.

In first step, we placed Region of interest (ROI) on the aorta to confirm a typical washout pattern. Subsequently, the enhancement curve was assessed in the initial phase and next in the late phase. In the T1 3D dynamic, the first two phases are the sequences that were used to assess the morphology of the lesion and to determine the inflow of contrast in the initial phase (where we defined the inflow as slow <50%, medium 50%–100%, and fast > 100%). The remaining acquisitions were used to determine the type of washout curve: type 1, benign; type 2, intermediate with plateau; type 3, malignant, with secondary washout.

In the dynamic sequence, ROI (size, 3 × 3 pixels) was measured three times on hyperintense lesions in DCE-MRI, both within mass and non-mass enhancement (NME). Lesion size was measured on the DCE MRI images. An apparent diffusion coefficient (ADC) was calculated from DWI by using a monoexponential model in dedicated and clinically validated software syngo.MR BreVis (Siemens Helthineers Erlangen Germany) using standardized

DWI preprocessing pipeline that included all necessary steps in particular epi-distortion and motion correction.

To determine the ADC value, we looked for pathological contrast enhancement—tumor mass or NME, which correlated with the hyperintensive region in the DWI (b = 800 s/mm^2) and the low signal on the ADC maps. Afterward, ROI about 5 ± 2 mm^2 was placed two times on the most restricted area inside the solid part of the lesion on the ADC map. We were trying to avoid cystic, necrotic, fatty regions, or hematoma after biopsy inside the mass using T2-weighted images or TIRM.

Statistical analysis

Quantitative data were reported as mean ± standard deviation (SD) or median/interquartile range, according to a normal distribution. For the qualitative data, frequencies and percentages were calculated. Mean differences between the two groups were compared by the Student's t-test, whereas the Mann–Whitney U-test was applied for comparisons of median values. The qualitative variables were compared using the chi-squared ($\chi 2$) test of proportions for categorical variables. The receiver operating characteristic (ROC) curves were used to assess both MRI and MMG method to better discriminate nodal status (presence of metastases based on US, widely regarded as the gold standard for tumor detection). Area under the curve (AUC) with standard error (SE) was reported, as well as sensitivity and specificity. In addition, the Spearman correlation between parameters was performed. Bland–Altman method was used to compare two radiological methods in measuring lesion size. The data were analyzed using StatSoft Statistica 13.1 PL for Microsoft Windows 10. The results with $P < 0.05$ were considered as statistically significant. Correspondence analysis was performed to compare the relative frequencies of prevalence of selected features across different imaging methods.

Results

Mammography

In a study group of 162 patients, 54 cases of tumor and 20 cases of high density areas were found (Table 1). The sensitivity of MMG in the diagnosis of ILC in the study group was 113 of the 162 (69.8%). Areas of high density identified by MMG most often did not correspond to morphological changes of the NME identified by MRI. Moreover, the size of the lesions found in the two methods was different ($P = 0.007$).

Ultrasound

In US, a mass was found in 144 of the 162 patients (mean size, 22.6 mm; range, 9–84 mm), and an area of indefinite shape and borders were detected in 17 patients (mean size, 28.6 mm; range, 10–87 mm). The sensitivity of US in the diagnosis of ILC in the study group was 161 of 162 (99.4%). The vast majority of changes (93.8%) revealed poorly defined contours. It was also discovered that areas of concern revealed by US do not correspond accordingly to NME morphological changes isolated by MRI.

Magnetic resonance imaging

In a study group of 162 patients with ILC, there were 113 tumors (69.8%) and 49 (30.2%) NME-type changes found in MRI. The most common morphological type of ILC was an irregular, spiculated mass showing heterogeneous contrast enhancement, diffusion restriction of the mean ADC value of 0.74 × 10–3 mm^2/s, and type III enhancement curve. In NME changes, the types of distribution most often found were focal (36.7%) and multi-regional (34.7%), with heterogeneous and clumped contrast enhancement accounting for 44.9% and 30.6%, respectively, of all NME changes. In NME changes, the dominant type of enhancement was type III with the mean ADC value of 0.72 × 10^3 mm^2/s (Table 1; Figures 1, 2).

Histopathology

The dominant type of tumor identified in histopathology was of grade (G feature) 2 (88.3%) with no amplification of HER2 receptors (92%). The mean value of receptor expression in the study group was, respectively, ER – 93.9% and PR – 58.7%, whereas the mean Ki67 value was 13.37%, which is related to the higher incidence of luminal A subtype in the study group (n = 97, 59.9%). The data on the mass feature G, structure, and background parenchymal enhancement (BPE) show that G2 tumors with heterogeneous fibroglandular structure and slight enhancement in the stroma are more common (Table 2; Figure 3).

Imaging and assessment of local extent

It is interesting that, in the study group, microcalcifications were found in 34 of 162 (21%) patients in MMG. In the group of changes presenting as tumors in MRI, microcalcifications were found in 20 of 113 (17.7%) patients in MMG, whereas in the NME group, they were significantly more often, i.e., found in 14 of 49 (28.6%) patients ($P < 0.05$).

The size of the lesions described in MRI did not differ significantly from those described by US examination ($P = 0.056$).

It has also been observed that the bigger the lesion, the higher the disproportion between its size measured in different methods: MRI *vs*. MMG $R = 0.455$; $P < 0.001$ and MRI *vs*. US $R = 0.425$; $P < 0.001$). The Bland–Altman plot along with scatterplot

10.3389/fonc.2022.855519

TABLE 1 Imaging parameters and clinicopathological features of 162 patients with invasive lobular carcinoma.

Demographic data					
Patients count		**162**			
Patients age (min/max/average)		**32/94/65.5**			
MRI: mass		**MRI: non-mass enhancement (NME)**		**MRI: other**	
Shape	**113**	**Distribution**	**49**	**Architectural distortion**	**162**
Oval	8	Focal	18	None	159
Round	4	Linear	4	Present	3
Irregular	101	Segmental	6	**Lymph nodes**	**162**
Margin	**113**	Regional	4	Normal	146
Circumscribed	8	Multiple regions	17	Abnormal	16
Not circumscribed	105	Diffuse	0		
Enhancement	**113**	**Enhancement**	**49**		
Homogeneous	28	Homogeneous	8		
Heterogeneous	81	Heterogeneous	22		
Rim enhancement	4	Clumped	15		
Dark internal septations	0	Clustered ring	4		
Kinetic curve (delayed phase)	**113**	**Kinetic curve (delayed phase)**	**49**		
Persistent	18	Persistent	8		
Plateau	34	Plateau	8		
Washout	61	Washout	33		
Mammography (MMG)Ultrasound (US)					
Lymph nodes	**162**			**Lymph nodes**	**162**
Normal	154			Normal	142
Abnormal	8			Abnormal	20
Findings	**74**			**Findings**	**161**
Mass	54			Mass	144
Asymmetric density	20			Region	17
Calcifications	**162**			**Margin**	**155**
None	128			Circumscribed	3
Present	34			Not circumscribed	152
Architectural distortion	**162**				
None	129				
Present	33				
Histopathology and immunohistochemistry					
Molecular subtypes	**162**			**Grading (G)**	**162**
Luminal A	97			G1	12
Luminal B (HER2−)	54			G2	143
Luminal B (HER2+)	9			G3	7
HER2 type	0				
Triple negative	2				

Comparison of results between three imaging modalities

		Total cases	**Average**	**Median**	**Min**	**Max**	**Std Dev**
Mass (mm)	MRI	**113**	35	30	5	122	24
	US		24	22	3	65	13
	MMG		24	20	1	84	15
NME (mm)	MRI	**49**	59	60.5	15	96	24
	US		31	26	0.9	84	18
	MMG		31	20.5	8	84	23

(Continued)

TABLE 1 Continued

Demographic data								
Patients count	**162**							
Patients age (min/max/average)	**32/94/65.5**							
MRI: mass	**MRI: non-mass enhancement (NME)**					**MRI: other**		
Receptors and markers statistics								
Tested positive	**Total cases**	**Average**	**Median**	**Min**	**Max**	**Low**	**Up**	**Std Dev**
Estrogen receptor ER (%)	162	93.97	100	0	100	90	100	15.14
Progesterone receptor PR (%)	162	58.70	75	0	100	8	100	41.07
Ki-67 biomarker (%)	162	13.37	10	0	70	5	20	11.11

graph is presented in Figure 4. The limits of agreement for the lesion measured in MRI and MMG varied from −59.68 to 23.84 mm and for MRI and US varied from −67.14 to 29.97 mm (Figure 4)

In the studied patients with T1 tumor found *via* US (n = 57), MRI showed that the size of the lesion was underestimated and the T feature of the lesion increased to T2 in 23 cases (41%) and to T3 in two cases (3.6%). A similar situation occurred in patients who had T2 tumor found in US (n = 92), and the lesion was reassessed as T3 in 35 cases (38%).

In 50 (30.8%) cases, MMG did not reveal any pathological changes (tumors, high-density areas, microcalcifications, and/or architectural alterations).

In the analyzed material, NME lesions were characterized by a higher range of sizes and were not as homogeneous as tumors.

Comparison of the ADC value and the tumor's T feature according to the TNM classification showed statistically significant difference between the T1 and T3 group of tumors. The higher the tumor's T feature, the lower the ADC value, which corresponds to increased diffusion restriction.

Architectural alterations were found in 20.4% of patients in MMG. Molecular studies revealed association on the verge of statistical significance between architectural alterations and increased expression of progesterone receptors (P = 0.57). Other results of molecular studies do not correlate with architectural alterations (Table 4). Architectural alterations found in MMG were confirmed in MRI in two patients only.

Imaging and molecular profile

Apart from the results presented here, no findings proved correlation between ILC presentation on imaging and molecular profile of the tumor. Microcalcifications did not correlate with

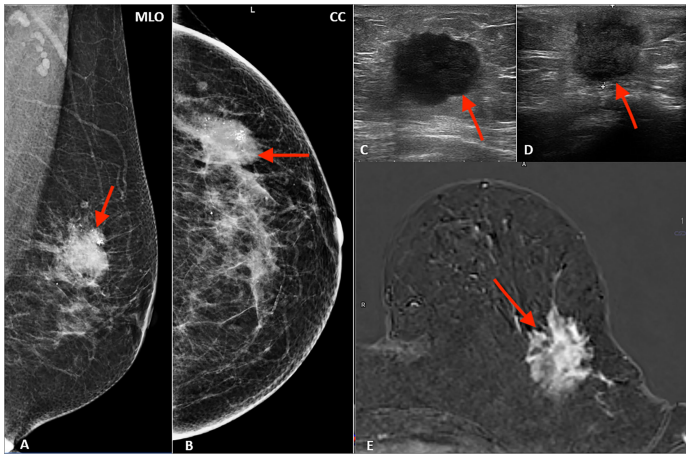

FIGURE 1
Multimodality presentation of lobular breast cancer; Patient 1 left breast: **(A, B)** mammography: MLO **(A)** and CC **(B)**—not circumscribed, spiculated mass with microcalcifications (red arrow); **(C, D)** ultrasound—not circumscribed, spiculated, hypoechoic mass (red arrow); **(E)** MRI T1 post contrast—not circumscribed, spiculated mass with heterogenous contrast enhancement (red arrow).

10.3389/fonc.2022.855519

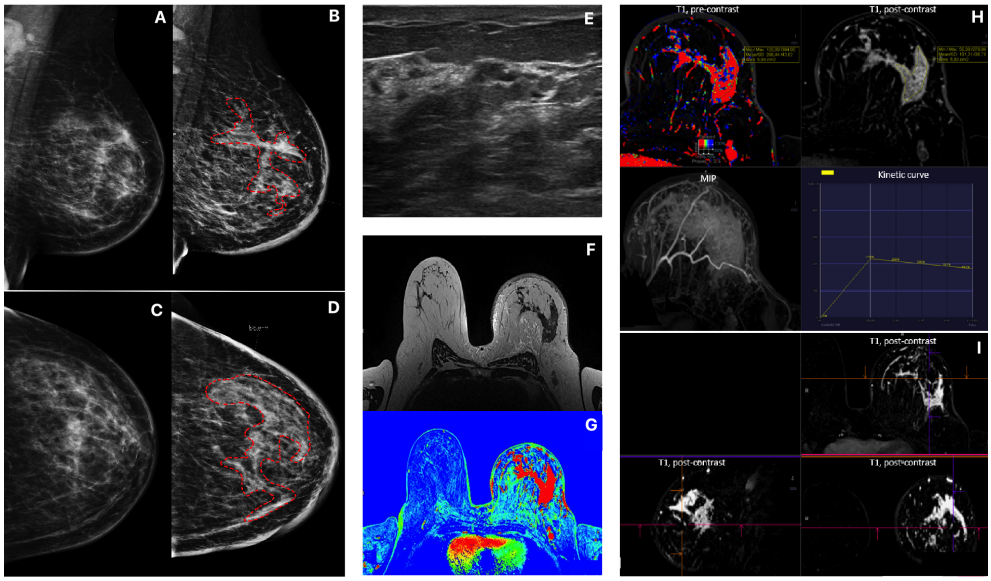

FIGURE 2
Patient 2, Multimodality presentation of Lobular Breast Cancer, left breast: **(A, B)** Mammography, [**(A)** MLO and **(B)** CC] asymetric density cancer, cancer marked with red dotted line. **(C, D)** Mammography, [**(C)** MLO and **(D)** CC] the same Patient after 4 months, cancer marked with red dotted line. **(E)** ultrasound- not circumscribed, hypoechoic region. **(F)** MRI T2 TSE - non-mass enhancement. **(G)** MRI T1 fl3d dynamic PEI. **(H, I)** MRI - diffused, non-mass enhancement with heterogenous enhancement [**(H)** T1 pre contrast; T1 post contrast; MIP and wash out kinetic curve; **(I)** 3D T1 post contrast].

the expression of HER2 receptors (P = 0.87), ER (P = 0.81), PR (P = 0.65), or Ki67 (P = 0.25). The same is true for architectural alterations that do not correlate with the expression of HER2 (P = 0.4), ER (P = 0.4), or Ki67 (P = 0.85). Similarly, morphological type of ILC revealed in MRI did not correlate with ADC value (P = 0.62) (Table 3).

Differences between luminal A and luminal B

In the study group consisting of 162 patients, there were 97 cases of luminal A subtype (59.9%), 54 cases of luminal B HER2– (33.3%), nine cases of luminal B HER2+ (5.5%), and two cases of

TABLE 2 Comparison between feature G *vs.* MRI and feature G *vs.* BPE.

Breast density	**G1**	**G2**	**G3**	**Total**
Almost entirely fat	2	19	0	21
Scattered fibrograndular tissue	4	77	4	85
Heterogenous fibrograndular tissue	4	36	2	42
Extreme fibrograndular tissue	2	11	1	14
Total	**12**	**143**	**7**	**162**
BPE	**G1**	**G2**	**G3**	**Total**
1. Minimal	6	68	4	78
2. Mild	1	37	1	39
3. Moderate	3	30	2	35
4. Marked	2	8	0	10
Total	**12**	**143**	**7**	**162**

10.3389/fonc.2022.855519

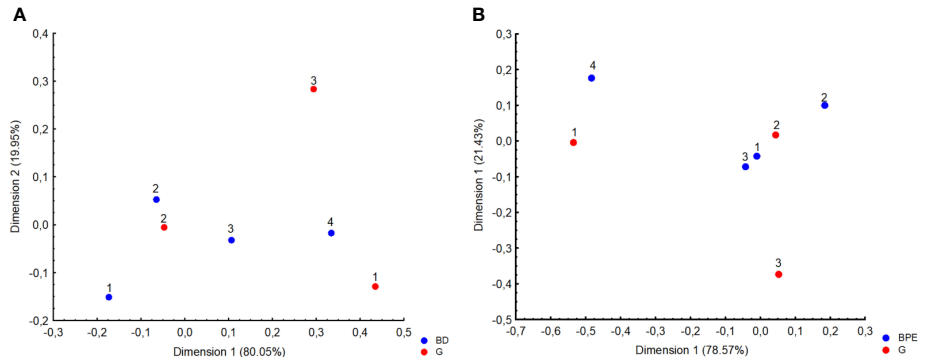

FIGURE 3
Correspondence analysis plot of the data which is a two-dimensional representation of grading (G) and **(A)** Breast Density (BD 1, almost entirely fat; 2, scattered fibrograndular tissue; 3, heterogenous fibrograndular tissue; 4, extreme fibrograndular tissue), as well as **(B)** background parenchymal enhancement (BPE).

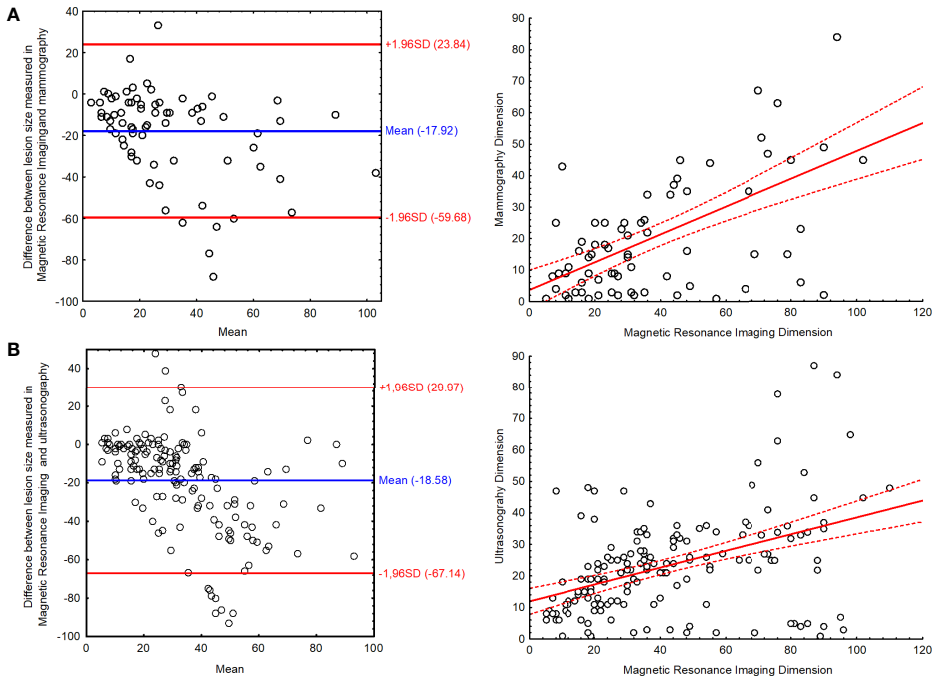

FIGURE 4
The Bland–Altman plot with scatter plot for the results of lesion size measured in magnetic resonance imaging and **(A)** mammography and **(B)** ultrasonography.

TABLE 3 Comparison between presence of microcalcifications and molecular tumor profile.

Variable	No Microcalcifications (n = 34)		Present Microcalcifications (n = 128)		
	Mean (SD)	Range	Mean (SD)	Range	p
ER	92.9	10–100	94.2	0–100	0.82
PR	55.1	0–100	59.6	10–100	0.66
KI67	14.6	1–60	13	5–19	0.26

triple negative (1.2%). The HER2 type was not found in the study group (Table 4).

Lymph nodes

In the study group, pathological lymph nodes were found in 20 patients (12.3%). US had the highest detection rate for pathological lymph nodes (US 12.3% vs. MRI 9.9% vs. MMG 4.9%) (MRI AUC 0.757 ± 0.071; MMG AUC 0.671 ± 0.076). MRI was shown to be more sensitive than MMG with similar specificity in imaging pathological nodes in patients with ILC when assessed using ROC curve (MRI sensitivity = 0.550; specificity = 0.965; MMG sensitivity = 0.350; specificity = 0.993) (Figure 5).

Discussion

Interestingly, this study confirms the findings of others regarding how MMG and US underestimate LBC size while MRI produces more accurate data. These findings suggest that MRI is the best choice during pre-operative management so as to customize the most appropriate therapeutic plan for the individual patient. (18–20) Some works suggest that ILC is often multifocal or even bilateral, but it is often not detected in methods other than MRI. Schelfout et al. demonstrated in their study that additional ILC foci, previously not shown by US or MMG, were detected in 50% of patients. (21) In addition to MRI's ability to most clearly define tumor parameters, this study also identified its ability to assess lesion size more accurately than other methods. This finding is important because

TABLE 4 Differences between luminal A and luminal B ILC type.

Demographic data

			Luminal A (Lum A)			**Luminal B (Lum B)**		
Patients count			97			63		
Patients age (min/max/average)			46/91/66			32/94/64.5		
General data								
Size distribution (feature T) in various methods		**T1size < 2 (cm)**	**T22 (cm) ≤ size < 5 (cm)**	**T3size ≥ 5 (cm)**	**Total cases**	**Grading (feature G)**	**Lum A**	**Lum B**
Lum A	MRI	22	45	30	97	G1	6	6
	MMG	78	16	3		G2	89	52
	US	45	46	6		G3	2	5
Lum B	MRI	14	28	21	63			
	MMG	40	19	4				
	US	25	35	3		Total cases	97	63
MRI: mass			**MRI: non-mass enhancement (NME)**			**MRI: other**		
	Lum A	**Lum B**		**Lum A**	**Lum B**		**Lum A**	**Lum B**
Shape			**Distribution**			**Architectural distortion**		
Oval	6	2	Focal	11	7	None	89	55
Round	3	1	Linear	3	1	Present	8	8
Irregular	56	43	Segmental	4	2	**FGT**		
Margin			Regional	3	1	Fat	14	6
Circumscribed	6	2	Multiple regions	11	6	Scattered	49	35
Not circumscribed	58	43	Diffuse	0	0	Heterogeneous	26	16
Spicular	1	1	**Enhancement**			Extreme	8	6
Enhancement			Homogeneous	4	4	BPE		
Homogeneous	22	5	Heterogeneous	15	7	Minimal	49	28
Heterogeneous	43	41	Clumped	10	5	Mild	21	18
Kinetic curve (delayed phase)			Clustered ring	3	1	Moderate	19	15
Persistent	15	3	**Kinetic curve (delayed phase)**			Marked	8	2
Plateau	17	16	Persistent	6	2			
Washout	33	27	Plateau	6	2			
			Washout	18	13			

(Continued)

TABLE 4 Continued

Mammography (MMG)	Lum A	Lum B
Calcifications		
None	78	48
Present	19	15
Architectural distortion		
None	77	50
Present	20	13
Lymph nodes		
Normal	94	58
Abnormal	3	5
Findings		
Mass	29	25
Asymm. density	11	9

Ultrasonography (US)	Lum A	Lum B
Margin		
Circumscribed	1	2
Not circumscribed	88	57
Irregular	4	1
Spicular	0	0
Lymph nodes		
Normal	86	54
Abnormal	11	9
Findings		
Mass	85	57
Region	11	6

Size and diffusion statistics

Characteristic			Total cases	Average	Median	Min	Max	Low	Up	Std Dev
mass MRI	Mass size (cm)	Lum A	65	3.41	2.80	0.50	9.80	1.80	4.50	2.31
		Lum B	46	3.66	3.10	0.60	12.20	1.80	4.40	2.68
	Mass ADC[10^{-3} mm^2/s]	Lum A	65	0.73	0.70	0.30	1.20	0.60	0.80	0.17
		Lum B	46	0.76	0.75	0.40	2.00	0.60	0.90	0.28
NME MRI	NME size (cm)	Lum A	32	5.82	5.55	2.00	11.00	3.60	8.05	2.60
		Lum B	17	6.24	7.10	1.50	9.00	4.40	8.30	2.35
	NME ADC[10^{-3} mm^2/s]	Lum A	32	0.74	0.72	0.00	1.20	0.60	0.87	0.24
		Lum B	17	0.68	0.70	0.30	1.20	0.50	0.70	0.23
MMG	Mass size (cm)	Lum A	29	1.65	1.10	0.10	8.40	0.50	2.20	1.73
		Lum B	25	3.03	2.50	0.10	8.40	1.50	4.50	1.98
	asymmetric density size (cm)	Lum A	11	1.52	0.80	0.10	6.70	0.20	1.60	1.99
		Lum B	9	1.48	1.10	0.20	4.40	0.30	1.60	1.51
US	mass size (cm)	Lum A	85	2.13	2.10	0.10	8.40	1.10	2.70	1.51
		Lum B	57	2.46	2.30	0.20	6.40	1.20	3.30	1.53
	region size (cm)	Lum A	11	2.85	2.80	0.10	5.60	2.20	3.70	1.59
		Lum B	6	2.90	1.95	0.10	8.70	1.30	3.40	3.05

this information affects the T feature of TNM classification and consequently changes therapeutic management. (22)

In addition, the image of ILC in MRI was the same as described in the literature. According to the authors, ILC presents most often as an irregular, spiculated tumor showing a washout enhancement curve type. However, one should remember that this picture is not pathognomonic for ILC and may correspond to invasive ductal carcinoma (IDC). (4, 18, 23)

One of the diagnostic problems described in the available literature is the determination of ADC value for NME changes. (24) It should be noted, however, that although the T feature of the tumor correlates with the ADC value obtained in MRI, the literature, the same as the presented study, does not show any association between molecular profile of the tumor and ADC value.14 Therefore, ADC value is suitable only to indicate potential malignancy of the tumor, but it cannot be used to predict its molecular profile when standard examination protocol is followed.

An MRI may present LBC in two forms: as a mass or NME. The percentage distribution of these changes in the described database is consistent with the data from the literature: – 5% to 69% for NME and 31% to 95% for the tumor. (25–28) In the study group, LBC most often appeared as a mass in MMG. The second most frequent manifestation of LBC was architectural alteration. The obtained results regarding the morphology of LBC in imaging are consistent with the data from the literature. (13, 29)

Moreover, some data from the literature suggest a high rate of false negative results in MMG, as high as 29% of ILC cases. (30) This finding is probably due to the fact that the only presentation of ILC in MMG may be architectural alterations without the mass. (31) Approximately 50 cases (30.8%) of our study group had tumors that were impossible to identify, as were their associated pathological areas. In the described study, architectural alterations found in MMG were not visible in MRI. One of the reasons for this invisibility is the structure of

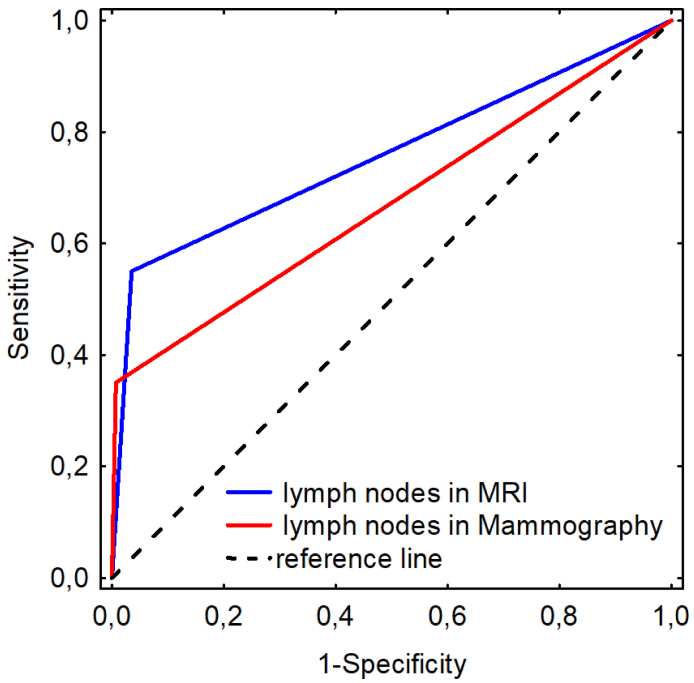

FIGURE 5
ROC curves for detecting lymph nodes in MRI and mammography.

breast tissue and it confirms that MRI is not a method of choice for the assessment of architectural alterations of the breast. (32)

Another factor that hinders the diagnosis of ILC in MMG is the relatively rare occurrence of microcalcifications. According to the literature, microcalcifications occur in only one to 25% of all ILC cases, which has a negative effect on the sensitivity of MMG in detecting this type of lesion (33–35). This finding is probably due to the fact that ILC does not invade milk ducts and, consequently, does not contribute to the formation of microcalcifications (13). At the same time, it should be noted that in the study group, microcalcifications were found in as many as in 42.85% of G3 tumors. It should be remembered, however, that there were too few patients with G3 tumor to consider these results statistically significant. The available literature indicates the much lower incidence of microcalcifications in ILC compared to IDC, which may be a predictive factor in the assessment of the tumor's G feature. This indication, however, requires further study on larger groups of patients (29).

In the study group, most LBC cases confirmed in MRI (99.38%) were also revealed in the US. Studies on the usefulness of US indicate its high sensitivity in the detection of LBC, defined by the authors at 68% to 95% (36–39). At the same time, the literature emphasizes the issue of accurate assessment of lesion size, an issue also highlighted in the presented work. The characteristics of LBC, particularly in this histological type of cancer, significantly complicate the assessment of the lesion borders and extent, which is often associated with underestimated size of the tumor (20, 40).

Literature mentions some attempts to find the association between radiological image and receptor profile of the tumor. Dilorenzo et al. reported attempts to demonstrate the relationship between BPE type and clinical tumor subtype. (41) This relationship, however, has not been found in the study group. Moreover, King et al. suggested in their work increased incidence of ILC in patients with high BPE. (42) Ko et al. found higher incidence of NME lesions in patients with the breast cancer (BC) HER2+ type (43).

Wen et al. correlated their findings with US images of the lesions. Interestingly, imaging did not reveal any differences between luminal A and luminal B morphologies, a finding consistent with ours. Wen et al. described the differences in the morphology between HER2-type tumors and the luminal type. Although the study by Wen et al. included a large number of study participants, none were experiencing HER2 tumors; therefore, data could not be compared between the study by Wen et al. and this one (44).

Despite the abovementioned limitations of US in the assessment of ILC size, it remains the gold standard in the diagnosis of changes in the lymph nodes. In the study group, US identified the largest number of pathological lymph nodes and was considered the gold standard in the evaluation of other methods (45, 46). The study is consistent with the literature data and it shows high sensitivity and specificity of MRI in the assessment of lymph nodes.

One limitation encountered during this study is the inability of MRI to correlate lesion size with its actual size as assessed *via* histopathology. This discrepancy was caused by retrospective methodology of the study and the fact that some patients received neoadjuvant chemotherapy that affected the size of the tumor before the surgery. As the result, objective determination of the lesion size in the histopathology was impossible. Historical evidence indicates that ILC is so rare and there is little archived data that describes it fully. Studies available for review are usually limited by any combination of these three elements: study limited to only one modality, group of study participants is small, or the histological type of BC is not taken into consideration (17, 47).

Conclusions

ILC poses a significant challenge to cancer diagnostics and management due to its histopathological and imaging complexity. This study strengthens the existing body of evidence, indicating that it is currently not possible to predict ILC molecular type when using imaging alone. Nevertheless, the large number of patients in this study made it possible to identify some radiological features that correlate to histopathology and part of the molecular panel. This study found MRI is still the preferred method for diagnosing ILC for multiple reasons that include how it enables detection of multifocal and bilateral neoplasms and allows for more reliable assessment of lesion size, both of which allow for improvements to therapeutic management plans based on TNM classification for ILC. Results obtained in the study group show, however, that there is no association between the studied parameters and proof that the morphology of ILC in imaging is independent of the cancer's histological type if luminal A and luminal B subtypes are considered. This study, like the study of Zhiqi Yang and Xiaofeng Chen (with others authors), suggests the importance of future study on larger groups of patients in multicenter settings as well as the value of developing radiogenetics, especially due to different results of studies (48).

Data availability statement

The original contributions presented in the study are included in the article/supplementary material. Further inquiries can be directed to the corresponding author/s.

Ethics statement

The study was conducted according to the Declaration of Helsinki. In each case an informed consent was obtained for all the procedures. All patients provided a written informed consent for the collection and publication of their medical data. Since the study was a retrospective analysis and did not involve any experimental interventions an independent ethics committee approval was abandoned. The Institutional Review Board reviewed and approved the study.

Author contributions

BD-K, ML, BS, and PK contributed to conception and design of the study. BD-K organized the database. MK performed the statistical analysis. BD-K and ML wrote the first draft of the manuscript. HM-J, MC, and MB wrote sections of the manuscript. All authors contributed to manuscript revision, read, and approved the submitted version.

Funding

This research was financed through statutory subsidies by the Minister of Science and Higher Education as part of the research grant SUBZ.C280.22.001 (record number in the Simple System).

Conflict of interest

The authors declare that the research was conducted in the absence of any commercial or financial relationships that could be construed as a potential conflict of interest.

Publisher's note

References

1. Montemezzi S, Camera L, Grazia M, Pozzetto A, Caliò A, Meliadò G, et al. Is there a correlation between 3T multiparametric MRI and molecular subtypes of breast cancer? *European Journal of Radiology* (2018) 108:120–7. doi: 10.1016/j.ejrad.2018.09.024

2. Derias M, Subramanian A, Allan S, Shah E, Teraifi HE, Howlett D. The role of magnetic resonance imaging in the investigation and management of invasive lobular carcinoma–a 3-year retrospective study in two district general hospitals. *Breast J* (2016) 22(4):384–9. doi: 10.1111/tbj.12594

3. Selvi V, Nori J, Meattini I, Francolini G, Morelli N, Di Benedetto D, et al. Role of magnetic resonance imaging in the preoperative staging and work-up of patients affected by invasive lobular carcinoma or invasive ductolobular carcinoma. *BioMed Res Int* (2018) 2018(Ilc):1–7. doi: 10.1155/2018/1569060

4. Lopez JK, Bassett LW. Invasive lobular carcinoma of the breast: Spectrum of mammographic, US, and MR imaging findings. *Radiographics* (2009) 29(1):165–76. doi: 10.1148/rg.291085100

5. Brem RF, Ioffe M, Rapelyea JA, Yost KG, Weigert JM, Bertrand ML, et al. Invasive lobular carcinoma: Detection with mammography, sonography, MRI, and breast-specific gamma imaging. *Am J Roentgenol* (2009) 192(2):379–83. doi: 10.2214/AJR.07.3827

6. Adachi Y, Ishiguro J, Kotani H, Hisada T, Ichikawa M, Gondo N, et al. Comparison of clinical outcomes between luminal invasive ductal carcinoma and luminal invasive lobular carcinoma. *BMC Cancer* (2016) 16(1):1–9. doi: 10.1186/s12885-016-2275-4

7. Ross JS, Slodkowska EA, Symmans WF, Pusztai L, Ravdin PM, Hortobagyi GN. The HER-2 receptor and breast cancer: Ten years of targeted anti–HER-2 therapy and personalized medicine. *Oncologist* (2009) 14(4):320–68. doi: 10.1634/theoncologist.2008-0230

8. Behjatnia B, Sim J, Apple SK. Does size matter? comparison study between MRI, gross , and microscopic tumor sizes in breast cancer in lumpectomy specimens. *Int J Clin Exp Pathol* (2010) 3(3):303–9.

9. Kuhl C, Kuhn W, Braun M, Schild H. Pre-operative staging of breast cancer with breast MRI: One step forward, two steps back? *Breast* (2007) 16(2 SUPPL.):34–44. doi: 10.1016/j.breast.2007.07.014

10. Barker SJ, Anderson E, Mullen R. Magnetic resonance imaging for invasive lobular carcinoma: is it worth it? *Gland Surgery* (2019) 8(3):237–41. doi: 10.21037/gs.2018.10.04

11. Cortadellas T, Argacha P, Acosta J, Rabasa J, Peiró R, Gomez M, et al. Estimation of tumor size in breast cancer comparing clinical examination, mammography, ultrasound and MRI-correlation with the pathological analysis of the surgical specimen. *Gland Surg* (2017) 6(4):330–5. doi: 10.21037/gs.2017.03.09

12. Arpino G, Bardou VJ, Clark GM, Elledge RM. Infiltrating lobular carcinoma of the breast: Tumor characteristics and clinical outcome. *Breast Cancer Res* (2004) 6(3):7–11. doi: 10.1186/bcr767

13. Hilleren DJ, Andersson IT, Lindholm K, Linnell FS. Invasive lobular carcinoma: Mammographic findings in a 10-year experience. *Radiology* (1991) 178(1):149–54. doi: 10.1148/radiology.178.1.1984294

14. Aydin H, Guner B, Bostanci IE, Bulut ZM, Aribas BK, Dogan L, et al. Is there any relationship between adc values of diffusion-weighted imaging and the histopathological prognostic factors of invasive ductal carcinoma? *Br J Radiol* (2018) 91(1084). doi: 10.1259/bjr.20170705

15. Horvat JV, Bernard-Davila B, Helbich TH, Zhang M, Morris EA, Thakur SB, et al. Diffusion-weighted imaging (DWI) with apparent diffusion coefficient (ADC) mapping as a quantitative imaging biomarker for prediction of immunohistochemical receptor status, proliferation rate, and molecular subtypes of breast cancer. *J Magn Reson Imag* (2019) 50(3):836–46. doi: 10.1002/jmri.26697

16. Jeh SK, Kim SH, Kim HS, Kang BJ, Jeong SH, Yim HW, et al. Correlation of the apparent diffusion coefficient value and dynamic magnetic resonance imaging findings with prognostic factors in invasive ductal carcinoma. *J Magn Reson Imag* (2011) 33(1):102–9. doi: 10.1002/jmri.22400

17. Navarro Vilar L, Alandete Germán SP, Medina García R, Blanc García E, Camarasa Lillo N, Vilar Samper J. MR imaging findings in molecular subtypes of breast cancer according to BIRADS system. *Breast J* (2017) 23(4):421–8. doi: 10.1111/tbj.12756

18. Mann RM, Hoogeveen YL, Blickman JG, Boetes C. MRI Compared to conventional diagnostic work-up in the detection and evaluation of invasive lobular carcinoma of the breast: A review of existing literature. *Breast Cancer Res Treat* (2008) 107(1):1–14. doi: 10.1007/s10549-007-9528-5

19. McGhan LJ, Wasif N, Gray RJ, Giurescu ME, Pizzitola VJ, Lorans R, et al. Use of preoperative magnetic resonance imaging for invasive lobular cancer: Good, better, but maybe not the best? *Ann Surg Oncol* (2010) 17(SUPPL.3):255–62. doi: 10.1245/s10434-010-1266-y

20. Boetes C, Veltman J, Van DL, Bult P, Wobbes T, Barentsz JO. The role of MRI in invasive lobular carcinoma. *Breast Cancer Res Treat* (2004) 86:31–37. doi: 10.1023/B:BREA.0000032921.10481.dc

21. Schelfout K, Van Goethem M, Kersschot E, Verslegers I, Biltjes I, Leyman P, et al. Preoperative breast MRI in patients with invasive lobular breast cancer. *Eur Radiol* (2004) 14(7):1209–16. doi: 10.1007/s00330-004-2275-7

22. Cuesta Cuesta AB, Martín Ríos MD, Noguero Meseguer MR, Velascod García JA, Martíneza MM, Sotillosa SB, et al. Accuracy of tumor size measurements performed by magnetic resonance, ultrasound and mammography, and their correlation with pathological size in primary breast cancer. *Cir Esp* (2019) 97(7):391–396. doi: 10.1016/j.ciresp.2019.04.017

23. Dietzel M, Baltzer PA, Vag T, Tobias G, Mieczyslaw G, Kaiser CO, et al. Magnetic resonance mammography of invasive lobular versus ductal carcinoma: Systematic comparison of 811 patients reveals high diagnostic accuracy irrespective of typing. *J Comput Assist Tomogr* (2010) 34(4):587–95. doi: 10.1097/RCT.0b013e3181db9f0e

24. Avendano D, Marino MA, Leithner D, Thakur S, Davila BB, Martinez DF, et al. Limited role of DWI with apparent diffusion coefficient mapping in breast lesions presenting as non-mass enhancement on dynamic contrast-enhanced MRI. *Breast Cancer Res* (2019) 21(1):1–10. doi: 10.1186/s13058-019-1208-y

25. Demard NF, Boulet P, Prat X, Charra L, Lesnik A, Taourel P. Breast MRI in invasive lobular carcinoma: Diagnosis and staging. *J Radiol* (2005) 86(9):1027–34. doi: 10.1016/s0221-0363(05)81487-8

26. Qayyum A, Birdwell RL, Daniel BL, Nowels KW, Jeffrey SS, Agoston TA, et al. MR imaging features of infiltrating lobular carcinoma of the breast: Histopathologic correlation. *Am J Roentgenol* (2002) 178:1227–32. doi: 10.2214/ajr.178.5.1781227

27. Rodenko GN, Harms SE, Pruneda JM, Farrell RS Jr, Evans WP, Copit DS, et al. MR imaging in the management before surgery of lobular carcinoma of the breast: Correlation with pathology. *Am J Roentgenol* (1996) 167:1415–19. doi: 10.2214/ajr.167.6.8956569

28. Yeh ED, Slanetz PJ, Edmister WB, Talele A, Monticciolo D, Kopans DB. Invasive lobular carcinoma: Spectrum of enhancement and morphology on magnetic resonance imaging. *Breast J* (2003) 9(1):13–18. doi: 10.1046/j.1524-4741.2003.09104.x

29. Savaridas SL, Bristow GD, Cox J. Invasive lobular cancer of the breast: A pictorial essay of imaging findings on mammography, sonography, and magnetic resonance imaging. *Can Assoc Radiol J* (2016) 67(3):263–76. doi: 10.1016/j.carj.2015.09.007

30. Porter AJ, Evans EB, Foxcroft LM, Simpson PT, Lakhani SR. Mammographic and ultrasound features of invasive lobular carcinoma of the breast. *Journal of Medical Imaging and Radiation Oncology* (2014) 58:1–10. doi: 10.1111/1754-9485.12080

31. Johnson K, Sarma D, Hwang ES. Lobular breast cancer series: imaging. *Breast Cancer Res* (2015) 2015:1–8. doi: 10.1186/s13058-015-0605-0

32. Gaur S, Dialani V, Slanetz PJ, Eisenberg RL. Architectural distortion of the breast. *Am J Roentgenol* (2013) 201:W662–W670. doi: 10.2214/AJR.12.10153

33. Krecke KN, Gisvold JJ. Invasive lobular carcinoma of the breast: Mammographic findings and extent of disease at diagnosis in 184 patients. *Am J Roentgenol* (1993) 161(5):957–60. doi: 10.2214/ajr.161.5.8273634

34. Le Gal M, Ollivier L, Asselain B, Meunier M, Laurent M, Vielh P, et al. Mammographic features of 455 invasive lobular carcinomas. *Radiology* (1992) 185(3). doi: 10.1148/radiology.185.3.1438749

35. Mendelson EB, Harris KM, Doshi N, Tobon H. Infiltrating lobular carcinoma: Mammographic patterns with pathologic correlation. *Am J Roentgenol* (1989) 153:265–71. doi: 10.2214/ajr.153.2.265

36. Berg WA, Gutierrez L, NessAiver MS, Carter WB, Bhargavan M, Lewis RS, et al. Diagnostic accuracy of mammography, clinical examination, US, and MR imaging in preoperative assessment of breast cancer. *Radiology* (2004) 233(3):830–49. doi: 10.1148/radiol.2333031484

37. Butler RS, Venta LA, Wiley EL, Ellis RL, Dempsey PJ, Rubin E. Sonographic evaluation of infiltrating lobular carcinoma. *Am J Roentgenol* (1999) 172:325–30. doi: 10.2214/ajr.172.2.9930776

38. Chapellier C, Balu-Maestro C, Bleuse A, Ettore F, Bruneton JN. Ultrasonography of invasive lobular carcinoma of the breast: Sonographic patterns and diagnostic value. report of 102 cases. *Clin Imag* (2000) 24(6):333–36. doi: 10.1016/S0899-7071(00)00234-5

39. Paramagul CP, Helvie MA, Adler DD. Invasive lobular carcinoma: Sonographic appearance and role of sonography in improving diagnostic sensitivity. *Radiology* (1995) 195(1):231–4. doi: 10.1148/radiology.195.1.7892476

40. Watermann DO, Tempfer C, Hefler LA, Parat C, Stickeler E. Ultrasound morphology of invasive lobular breast cancer is different compared with other types of breast cancer. *Ultrasound Med Biol* (2005) 31(2):167–174. doi: 10.1016/j.ultrasmedbio.2004.11.005

41. Dilorenzo G, Telegrafo M, La Forgia D, Stabile Ianora AA, Moschetta M. Breast MRI background parenchymal enhancement as an imaging bridge to molecular cancer sub-type. *Eur J Radiol* (2019) 113:148–52. doi: 10.1016/j.ejrad.2019.02.018

42. King V, Brooks JD, Bernstein JL, Reiner AS, Pike MC, Morris EA. Background parenchymal enhancement at breast MR imaging and breast cancer risk. *Radiology* (2011) 260(1):50–60. doi: 10.1148/radiol.11102156

43. Ko ES, Lee BH, Kim HA, Noh WC, Kim MS, Lee SA. Triple-negative breast cancer: Correlation between imaging and pathological findings. *Eur Radiol* (2010) 20:1111–17. doi: 10.1007/s00330-009-1656-3

44. Azim HA, Malek RA, Azim HA. Pathological features and prognosis of lobular carcinoma in Egyptian breast cancer patients. *Women's Heal* (2014) 10 (5):511–8. doi: 10.2217/whe.14.48

45. Oliveira TMG, Elias J, Melo AF, Teixeira SR, Filho SC, Gonçalves LM, et al. Evolving concepts in breast lobular neoplasia and invasive lobular carcinoma, and their impact on imaging methods. *Insights Imag* (2014) 5(2):183–94. doi: 10.1007/s13244-014-0324-6

46. Adejolu M, Krishnamurthy S, Whitman GJ. Ultrasound of invasive lobular carcinoma. *Ultrasound Clin* (2011) 6(3):313–25. doi: 10.1016/j.cult.2011.04.002

47. Wen X, Yu Y, Yu X, Cheng W, Wang Z, Liu L, et al. Correlations between ultrasonographic findings of invasive lobular carcinoma of the breast and intrinsic subtypes. *Ultraschall Med* (2019) 40(06):764–70. Korrelation der sonografischen Befunde des invasiven lobulären Mammakarzinoms und der intrinsischen Subtypen Patients with ILC. doi: 10.1055/a-0715-1668

48. Zhiqi Y, Chen X, Zhang T, Cheng F, Liao X, Chen X, et al. Quantitative multiparametric MRI as an imaging biomarker for the prediction of breast cancer receptor status and molecular subtypes. *Front. Oncol* (2021). doi: 10.3389/fonc.2021.628824